This is an open access article published under a Creative Commons Non-Commercial No Derivative Works (CC-BY-NC-ND) Attribution License, which permits copying and redistribution of the article, and creation of adaptations, all for non-commercial purposes.

ACS AUTHORCHOICE

CHEMISTRY OF MATERIALS

Article

Cite This: Chem. Mater. 2020, 32, 557−565

pubs.acs.org/cm

Locating and Controlling the Zn Content in In(Zn)P Quantum Dots

Nicholas Kirkwood,*[,†,▽] Annick De Backer,[‡] Thomas Altantzis,[‡] Naomi Winckelmans,[‡] Alessandro Longo,[§,∥] Felipe V. Antolinez,[⊥] Freddy T. Rabouw,[⊥,○] Luca De Trizio,[#] Jaco J. Geuchies,[†] Jence T. Mulder,[†] Nicolas Renaud,[†,◆] Sara Bals,[‡] Liberato Manna,[#] and Arjan J. Houtepen*[,†]

[†]Opto-Electronic Materials Section, Faculty of Applied Sciences, Delft University of Technology, Van der Maasweg 9, 2629 HZ Delft, The Netherlands

[‡]EMAT, University of Antwerp, 2020 Antwerp, Belgium

[§]XMI, Department of Chemistry, Ghent University, Krijgslaan 281 S12, Ghent, East Flanders 9000, Belgium

[∥]Istituto per lo Studio dei Materiali Nanostrutturati (ISMN)-CNR, UOS Palermo, Via Ugo La Malfa, 153, 90146 Palermo, Italy

[⊥]Optical Materials Engineering Laboratory, Department of Mechanical and Process Engineering, ETH Zurich, 8092 Zurich, Switzerland

[#]Department of Nanochemistry, Istituto Italiano di Tecnologia (IIT), Via Morego, 30, 16163 Genova, Italy

Supporting Information

ABSTRACT: Zinc is routinely employed in the synthesis of InP quantum dots (QDs) to improve the photoluminescence efficiency and carrier mobility of the resulting In(Zn)P alloy nanostructures. The exact location of Zn in the final structures and the mechanism by which it enhances the optoelectronic properties of the QDs are debated. We use synchrotron X-ray absorbance spectroscopy to show that the majority of Zn in In(Zn)P QDs is located at their surface as Zn carboxylates. However, a small amount of Zn is present inside the bulk of the QDs with the consequent contraction of their lattice, as confirmed by combining high-resolution high-angle annular dark-field imaging scanning transmission electron microscopy with statistical parameter estimation theory. We further demonstrate that the Zn content and its incorporation into the QDs can be tuned by the ligation of commonly employed Zn carboxylate precursors: the use of highly reactive Zn acetate leads to the formation of undesired Zn_3P_2 and the final nanostructures being characterized by broad optical features, whereas Zn carboxylates with longer carbon chains lead to InP crystals with much lower zinc content and narrow optical features. These results can explain the differences between structural and optical properties of In(Zn)P samples reported across the literature and provide a rational method to tune the amount of Zn in InP nanocrystals and to drive the incorporation of Zn either as surface Zn carboxylate, as a substitutional dopant inside the InP crystal lattice, or even predominantly as Zn_3P_2.

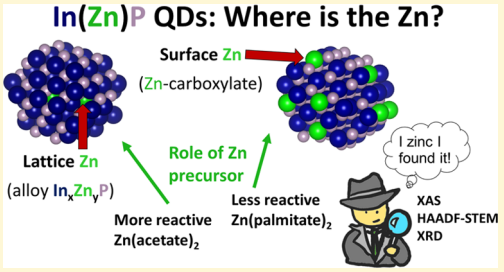

INTRODUCTION

Indium phosphide quantum dots (QDs) are a promising replacement material for Cd-based QDs in applications where the use of highly toxic Cd is regulated or prohibited. To meet the performance requirements for many optoelectronic applications, zinc is commonly added to the synthesis of InP QD reactions as it is found to increase the photoluminescence quantum yield (PL QY) and stability of the resulting In(Zn)P QDs.[1−3] However, readily achievable PL QYs for In(Zn)P-based QDs are typically around 70−90%, with PL full width at half maxima (FWHM) of 36−70 nm.[4−9] This leaves much room for improvement compared to Cd-based QDs, which readily reach PL QYs over 90% and PL FWHM values below 30 nm.[10,11] The development of ideal In(Zn)P QDs is at least partly hindered by the lack of a consensus in the literature regarding the location of the added zinc atoms, and consequently, the mechanism by which Zn enhances the optoelectronic properties of InP QDs is not well understood.

In this work, we address the question of Zn location in In(Zn)P QDs, focusing on the well-studied reaction system involving the injection of tris(trimethylsilyl)phosphine (PTMS) into a solution of indium and zinc carboxylates in octadecene (ODE) at ∼300 °C.[1,12] The effects we have reported previously of Zn on the optical, compositional, and structural properties of InP QDs produced by this reaction system are summarized in Figure 1. There is a blue-shift of the absorbance (Figure 1A) and PL (Figure 1B) with an increasing amount of zinc in the synthesis, which reverts to a red-shift for high Zn loadings (feed Zn/In ratios, >1), accompanied by a broadening of the optical features. The measured Zn/In ratio (from atomic emission spectroscopy) in washed QDs increases

Received: October 28, 2019
Revised: December 12, 2019
Published: December 13, 2019

Downloaded via UTRECHT UNIV on March 16, 2021 at 16:01:15 (UTC).
See https://pubs.acs.org/sharingguidelines for options on how to legitimately share published articles.

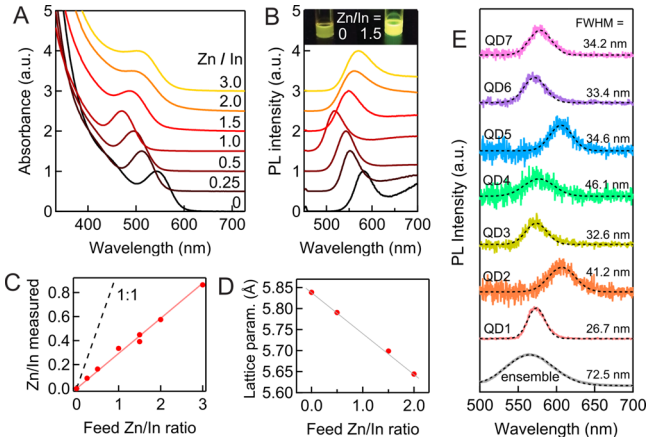

Figure 1. Effect of increasing Zn/In feed ratio on In(Zn)P QD synthesis (0.12 mmol of $In(OAc)_3$, 0.36 mmol of HPA, 0.06 mmol of PTMS, injection at 300 °C, and growth for 1 h at 270 °C). (A) Normalized absorbance and (B) PL spectra of In(Zn)P QDs with increasing Zn added to the reaction, giving feed Zn/In molar ratios from 0 to 3. Photo at the top shows PL under UV light for Zn/In = 0 and 1.5 samples. (C) Measured Zn/In molar ratio (ICP) of washed In(Zn)P samples as a function of Zn/In feed molar ratio on the same samples after thorough washing. The red line is a linear fit passing through the origin with a gradient of 0.293. The dashed black line shows a gradient of 1, that is, 100% incorporation of Zn into QDs. (D) Lattice parameter of In(Zn)P QDs as a function of Zn/In feed ratio (measured from XRD) showing lattice contraction with increasing Zn content. The line is a guide to the eye. (E) Ensemble PL spectrum of In(Zn)P/ZnS QDs (Zn/In = 1.5) and single particle PL spectra of different QDs in the sample (QD1–QD7). The spectra have been normalized, and the FWHM value for each spectrum is marked on the right, determined by a Gaussian fit (dashed lines).

linearly with the feed Zn/In ratio (Figure 1C), confirming that Zn is within or tightly bound to these QDs.[3]

Crucially, the band-edge PL intensity also increases with Zn added during the InP reaction, and some groups have concluded that this is because Zn is entirely located at the QD surface, where it passivates surface traps.[1] Indeed, Stein and co-workers[13] observed PL increases when treating pure InP QDs with zinc salts post synthesis, which is indicative of surface trap passivation. This conclusion does not however explain the observed spectral shifts and broadening when zinc is added at the beginning of the reaction (Figure 1A,B). Furthermore, X-ray diffraction (XRD) measurements show a lattice contraction that is greater with increasing pre-added Zn content (Figure 1D), consistent with the formation of Zn–P bonds inside the QD that are shorter than In–P bonds.[3,6] These observations led us to conclude that pre-added Zn is likely incorporated in the QD as a substitutional dopant, forming a higher-bandgap In_xZn_yP material (hence, the initial blue-shift in the PL), which could be lattice-matched to a $ZnSe_yS_{1-y}$ shell material to increase the final PL QY.[3] Other groups have shown that a complex containing Zn–P bonds is a key intermediate in the formation of crystalline InP QDs, suggesting a plausible mechanism for the inclusion of Zn in the crystal.[14]

It is conceivable that the use of Zn in the synthesis leads to an inhomogeneous inclusion of Zn in the QDs and, consequently, to a distribution of QDs differing from each other in terms of emission energy. Recently, Janke et al.[15] provided experimental X-ray absorbance evidence for this idea. They further proposed, based on DFT calculations, that substitutional Zn presents an in-gap state in InP QDs, which quickly captures photogenerated holes. Indeed, substitutional Zn is a well-known shallow acceptor within bulk InP with an ionization energy of 35 meV.[16−18] The observed broad emission could be the result of recombination between a delocalized conduction band electron and a hole localized on the interstitial Zn. The broad emission would result both from strong electron–phonon coupling and sample-to-sample variations in the position and amount of Zn atoms in the QD.[15]

To elucidate this point, we acquired single-particle PL spectra (see the Experimental Section) of In(Zn)P/ZnS QD samples (Zn/In = 1.5, see Figure 1E), which evidence that individual QDs have highly variable PL energies, as well as variable PL linewidths (FWHM, 27–46 nm) that are narrower than that from the ensemble (FWHM, 73 nm). We note that the narrowest linewidths observed are still significantly broader than those observed for CdSe/CdS/ZnS QDs (100 meV vs ~50 meV),[10,19] which could indicate that the emission indeed involves recombination of electrons with holes localized on Zn, as suggested by Janke et al.[15] The large variation in single-QD PL linewidth can also be explained by this model as the strength of electron–phonon coupling, as well as the associated broadening of the PL, likely depends on the amount and location of Zn ions in the lattice. Regardless of the exact nature of the emission process, it is clear that a better control over the process of incorporation of Zn into InP QDs could lead to much improved ensemble linewidths. This further motivates the need to understand the location of Zn at the atomistic level.

Here, we use a combination of synchrotron X-ray absorbance spectroscopy and ligand removal techniques to show that, for a typical In(Zn)P synthesis, the large majority of Zn atoms are bound to the QD surface as Zn carboxylate species. In addition, high-angle annular dark-field scanning transmission electron microscopy (HAADF-STEM) data combined with statistical parameter estimation theory[20] indicate lattice contractions for some of the investigated QDs, in agreement with the XRD measurements. This suggests that a small amount of zinc is indeed present in the bulk of the QDs. Furthermore, we show that the identity of the Zn carboxylate precursors employed in the synthesis determines the location and the amount of Zn that is incorporated into the QDs: by decreasing the chain length of the Zn carboxylates, an increased incorporation of Zn inside the core of the InP nanocrystals is observed, with the extreme case being the use of Zn acetate that can lead to evidence of Zn_3P_2 crystal domains and significant optical broadening. Finally, we discuss how variations in the preparation techniques used for Zn carboxylates (or other Zn compounds) across the literature may be the cause of significant deviations regarding the location and effect of Zn in the resulting In(Zn)P QDs.

RESULTS AND DISCUSSION

Location of Zn from X-ray Absorbance Measurements. We set out to determine the location of zinc in In(Zn)P QDs using synchrotron extended X-ray absorbance fine structure spectroscopy (EXAFS) measurements, a technique that can provide information on the chemical and structural environment around the absorber atom (in this case, Zn).[21] The first analyzed sample consisted of In(Zn)P QDs synthesized via the in situ precursor method,[7] in which In and Zn carboxylates are generated in situ from the reaction of

DOI: 10.1021/acs.chemmater.9b04407
Chem. Mater. 2020, 32, 557−565

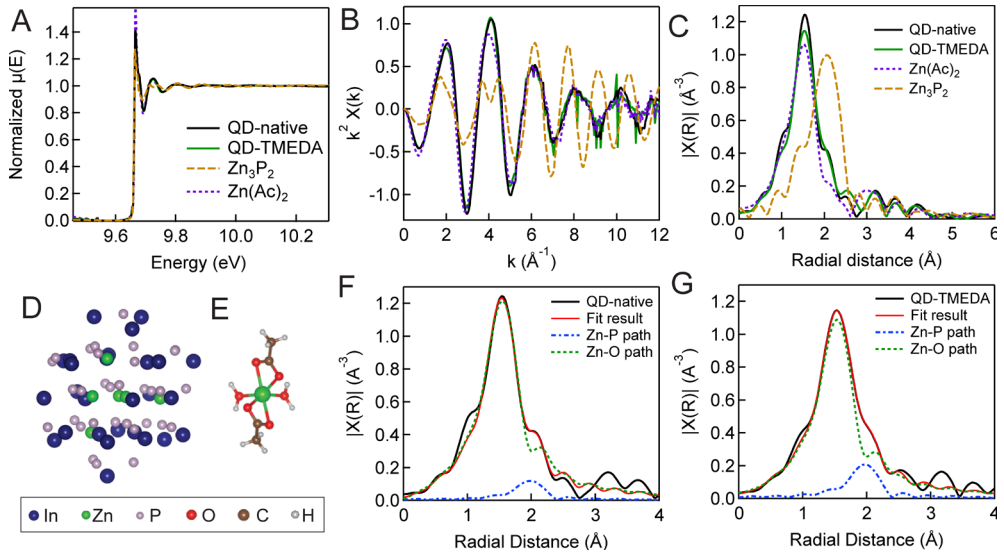

Figure 2. Zn K-edge EXAFS analysis of In(Zn)P QDs. (A) Normalized XAS signals, μ(E), for native In(Zn)P QDs (QD-native, black), In(Zn)P QDs treated with TMEDA (QD-TMEDA, green), zinc acetate dihydrate (purple dashed), and zinc phosphate (dark yellow dashed). (B) k^2-weighted X(k) EXAFS data extracted from μ(E) by removal of a background spline (see the Experimental Section for details, legend as per (A)). (C) |X(R)|, the Fourier transform magnitude (k^2-weighted) of EXAFS data for the same samples. (D) DFT-minimized model of 1.45 nm InZnP cluster (hydrogen-passivated) with six substitutional Zn atoms ($In_{28}Zn_6P_{32}H_{66}$). For clarity, hydrogen atoms are not shown. (E) Zinc acetate dihydrate structure from the COD database (#2006420). (F, G) Quantitative fits to R-space (k^2-weighted) profiles of QD-native (F) and QD-TMEDA (G) samples using one Zn−O scattering path from the zinc acetate structure in (C) and one Zn−P scattering path calculated from the $In_{28}Zn_6P_{32}H_{66}$ cluster in (B) (see the Experimental Section for details).

In and Zn acetates with palmitic acid (see the Experimental Section) using a Zn/In feed ratio of 1.5. ICP measurements on In(Zn)P QDs indicated a final Zn/In ratio of 0.392 after washing (see Figure 1C), and in line with previous reports, the lattice parameter measured using XRD was smaller than for Zn-free InP QDs (see Figure 1D).

To differentiate between possible surface and bulk Zn species, we further attempted to strip the native ligands from the In(Zn)P QDs by suspending the QDs in a solution of neat tetramethylenediamine (TMEDA) at 50 °C for 24 h, a technique that has been shown for CdSe QDs to remove almost all Z-type metal carboxylate ligands while retaining their colloidal stability.[22] Following precipitation of the QDs from the TMEDA solution by addition of methyl acetate, the ligand-rich supernatant exhibited a Zn/In ratio of 11.8 from ICP measurements, confirming that there was a substantial excess of Zn on the QD surface. The Zn/In ratio of the resulting QDs that were washed three times with methyl acetate dropped to 0.197. On the other hand, XRD diffractograms of In(Zn)P QDs before and after the ligand stripping procedure with TMEDA were identical (see Figure S1, Supporting Information), indicating no structural changes. These preliminary results indicate that the Zn species removed during the TMEDA treatment came from the surface of the QDs.

Figure 2A shows the normalized X-ray absorbance (μ(E)) of the Zn K-edge EXAFS measurements on solutions of washed In(Zn)P QDs with native ligands (QD-native, black line) and after the ligand stripping with TMEDA (QD-TMEDA, green line), as well as for zinc acetate in ethanol (purple dashed line) and a bulk Zn_3P_2 powder (dark yellow dashed line). By subtraction of a background spline and Fourier processing according to standard protocols using the Athena software[23] (see Table S1, Supporting Information), the k^2-weighted EXAFS signal k^2X(k) (Figure 2B) and the magnitude of the Fourier-transformed EXAFS signal |X(R)| (k^2-weighted, Figure 2C) were obtained. The |X(R)| plots in Figure 2C show a strong peak at a radius R related to backscattering of emitted photoelectrons with the nearest neighbors (first coordination shell) of the absorber atom (Zn); hence, Zn_3P_2 (Zn−P bond length, ∼2.4 Å) has a peak at higher R values than zinc acetate (Zn−O bond length, ∼2.0 Å). The difference between the peak positions in Figure 2 and the actual bond lengths is due to a phase shift in the scattering process.[21]

The EXAFS data of both QD samples (i.e., QD-native and QD-TMEDA) closely resemble that of the zinc acetate solution, although the radial profile of both QD samples differs from zinc acetate at higher radial distances. To better understand the EXAFS results of the QD samples and the actual effects of the TMEDA treatment, we also measured the EXAFS absorbance of the TMEDA−ligand supernatant solution, whose profile was consistent with that expected for TMEDA−Zn complexes (see Figure S2, Supporting Information). This measurement indicated that the change in EXAFS signals between the QD-TMEDA and QD-native samples is due to the removal of Zn-containing ligands.

To decompose the experimental EXAFS data into contributions from Zn−P coordination (from Zn inside the QD) and Zn−O coordination (from surface Zn acetate), we fit the QD EXAFS data using a first coordination shell comprised of Zn−P and Zn−O scattering paths. Scattering paths were calculated from crystal structures using the "IFEFFIT" code[24] and fit to EXAFS data with the Artemis software package.[23] To simulate the Zn−P scattering path expected for a Zn-doped InP QD, we used an IFEFFIT aggregate calculation of all Zn atoms in a density functional theory (DFT)-minimized, 1.45 nm-diameter In−Zn−P cluster with six substitutional Zn atoms ($In_{28}Zn_6P_{32}H_{66}$, see Figure 2D). The Zn−O scattering path was taken from the primary Zn−O single scattering path in zinc acetate dihydrate (Crystallography Online Database #2006420, see Figure 2E).

DOI: 10.1021/acs.chemmater.9b04407
Chem. Mater. 2020, 32, 557−565

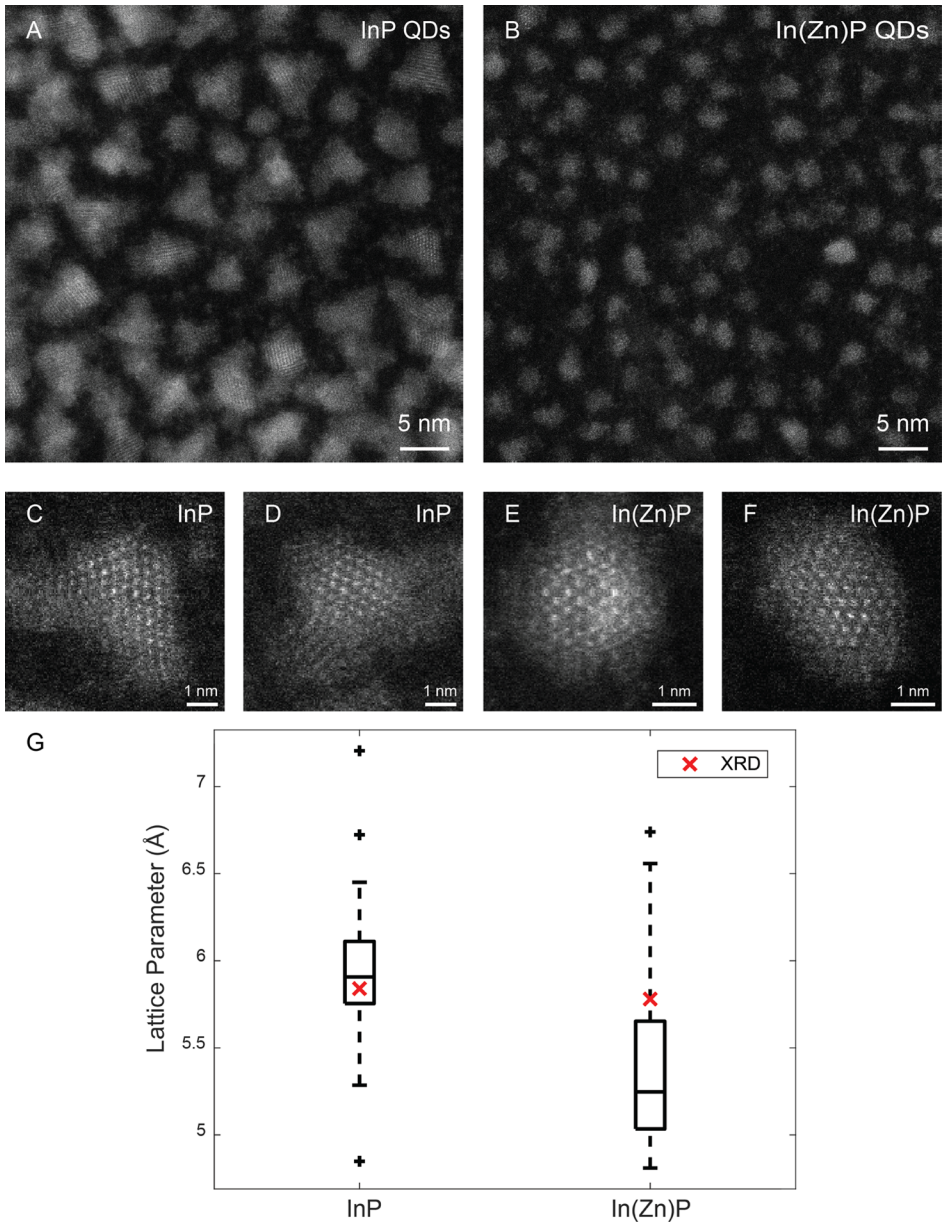

Figure 3. Structural characterization of InP and In(Zn)P QDs using HAADF-STEM. (A, B) Overview images of the InP and In(Zn)P QDs, respectively. (C, D) Atomic-resolution HAADF-STEM images of InP QDs. (E, F) Atomic-resolution HAADF-STEM images of In(Zn)P QDs. (G) Box-and-whisker plots showing the average and range of lattice parameters from InP and In(Zn)P QDs in comparison to the lattice parameters for same QD ensemble measured from XRD (red crosses).

The QD sample $|X(R)|$ plots are shown as black lines in Figure 2F (QD-native) and Figure 2G (QD-TMEDA) along with the fit results (red lines, fit window R = 1 to 3 Å) and the contribution to the fit of the Zn−O scattering path (green dashed lines) and the Zn−P scatter path (blue dashed lines). Plots of the fits against $k^2X(k)$ and $\mathrm{Re}[X(R)]$, as well as detailed summaries of all fit parameters, are available in Figures S3−S7 (Supporting Information). Of particular importance, the amplitude of each path in Figure 2F,G is defined by a fitted coordination number (CN), which can be considered as the relative contribution of that path to the fit. To fit the EXAFS profile of the QD-native sample, a large contribution from the Zn−O path (CN = 3.62) and a small contribution from the Zn−P path (CN = 0.28) were obtained (ratio CN(Zn−P)/CN(Zn−O) = 0.077). On the other hand, for the QD-TMEDA sample, a higher contribution of the Zn−P path was obtained (ratio CN(Zn−P)/CN(Zn−O) = 0.092). In both cases, the Zn−P path was necessary to improve the fit around R = 2 Å (see Figures S4 and S6, Supporting Information, for fit results without the Zn−P paths).

These results show clearly that the majority of Zn ions in In(Zn)P samples reside on the surface of the QDs as Zn carboxylate ligands, even after the treatment with TMEDA. The presence of some Zn−P bond lengths is not surprising as even Zn carboxylate ligands are expected to be bound to surface phosphorus; indeed, the low observed CN for Zn−P scattering paths implies that the surface phosphorus is likely oxidized,[25−27] and the Zn carboxylate may bind to the oxygen rather than phosphorus. However, the relative increase in Zn−P CN after ligand removal (Figure 2G) provides tentative support for the conclusion that some of the Zn−P signals come from Zn bound to P within the QD. If Zn was present only on

DOI: 10.1021/acs.chemmater.9b04407
Chem. Mater. 2020, 32, 557−565

the surface of the QDs (with Zn carboxylate ligands bound to surface phosphorus), the relative number of Zn−P and Zn−O bonds should remain constant irrespective of how many ligands are bound.

Direct Observation of Lattice Contraction from HAADF-STEM Images. In our previous work,[3] one of the proofs we used to support the formation of alloyed In(Zn)P QDs was the systematic lattice contraction, measured by using X-ray diffraction, which was observed upon the progressive increase of the Zn precursor in the synthesis of InP QDs. In light of the EXAFS data discussed above, which suggest that Zn inside the QDs must be present only in small quantities, we set out to more rigorously test this lattice contraction by employing HAADF-STEM (Figure 3). Due to the high sensitivity the QDs exhibit under prolonged exposure to the electron beam, local energy dispersive X-ray spectroscopy (EDXS) mapping was not able to provide conclusive evidence regarding the location of Zn. However, by using statistical parameter estimation theory, we were able to extract structure parameters from the HAADF-STEM images[20,28] and therefore directly measure the projected lattice parameter at the core of the QDs. To increase the measurement accuracy, we grew larger InP QDs (4.7 nm in diameter) via injection of extra precursors after the hot injection process (see the Experimental Section). For In(Zn)P QDs, a single injection of precursor was used (QD diameter, 3.0 nm) as we found that, after the initial hot injection process, the subsequently added Zn precursor does not seem to be readily incorporated into the QDs as the QDs grow larger (see Table S2, Supporting Information).

Results were obtained by analyzing different QDs (see Figures S9 and S10), and we observed a broader range of lattice parameters in In(Zn)P QDs compared to InP, as well as a contraction in the average lattice parameter in In(Zn)P QDs (see Figure 3C and Table 1). This reinforces our earlier conclusions based on XRD results[3] and, combined with evidence of a bulk Zn−P signal in the EXAFS results, points toward the incorporation of a small amount of Zn into the QDs. Since the characterization using HAADF-STEM provides local information for the different QDs, the broader range of the measured lattice parameters for the In(Zn)P QDs (see Figure S11) suggests that Zn is not always incorporated in the QDs, and if it is, it is not present in a specific amount.

Table 1. Zn/In Ratios and Measured Lattice Parameters of In(Zn)P Samples Used for HAADF-STEM Experiments

feed Zn/In	QD diameter (51 particles)	Zn/In (ICP)	Zn/In (EDXS)	lattice parameter from STEM (Å)	lattice parameter from XRD (Å)
0	4.66 ± 0.09	0	0	5.93 ± 0.06	5.84
1.5	2.96 ± 0.06	0.448	0.22	5.38 ± 0.07	5.78

We have previously argued that this lattice contraction is best explained by the presence of Zn within the InP crystal, that is, the formation of an In_xZn_yP alloy. However, the results from this work show that any Zn within the QD must be in far lower quantities than the surface-bound zinc carboxylate species that dominate the signal in EXAFS data (Figure 2). Our current findings thus resolve the contradiction posed by the observation of a very high content of Zn in In(Zn)P QDs prepared with high Zn/In feed ratios (e.g., nearly 50% zinc for a feed Zn/In ratio of 1.5), which would imply that the material is as much zinc phosphide as indium phosphide. The actual situation, as demonstrated here, is that, under typical reaction conditions, only a small amount of zinc is incorporated in the lattice of the QDs, leading to a contraction of their crystal structure, while the remainder serves as a Z-type surface ligand in the form of Zn carboxylates.

Controlling the Zinc Content and Location. We now turn to discussing factors that can control the amount and location of Zn incorporated into In(Zn)P QDs and, in particular, how this can explain disagreements regarding these points across the literature. Considering the results/findings shown so far, what we expect is that the Zn/In ratio measured for different In(Zn)P samples across the literature will vary depending on the QD ligand surface coverage as the main contribution to the amount of Zn comes from surface Zn carboxylates. A first discrepancy, for example, can be found by comparing the results of this work with those we reported in an earlier publication:[3] the slope of the "measured Zn/In versus feed Zn/In molar ratios" plot in this work is ∼0.3 (red line in Figure 1C), while previously,[3] we found a gradient of 1 (dashed line in Figure 1C). The only obvious procedural difference between these two works is the washing procedure: originally, we used an ethanol/acetone mixture as the antisolvent for the precipitation of the QDs,[3] but for this work, we employed methyl acetate. The different ability of these solvents to strip surface Zn carboxylates[22,29] could have resulted in In(Zn)P NC samples having a different surface coverage, that is, a different measured Zn/In ratio. We however measure a similar lattice contraction as in our previous work (for the same Zn/In ratio),[3] suggesting that the Zn causing lattice contractions is not removed by washing.

Perhaps more importantly, our EXAFS results indicate that only a minor fraction of Zn was incorporated into the lattice of InP QDs; this in some disagreement with similar measurements on In(Zn)P QDs by Janke et al.,[15] who concluded from Zn K-edge measurements that the Zn in their QDs was primarily bonded to P within the crystals. Indeed, our findings more closely resemble those of Stein et al.[13] who treated pure InP QDs with Zn carboxylates post synthesis and used EXAFS to conclude that all of the Zn was located on the surface as carboxylates. However, as the Zn in our reactions is added prior to nucleation, we expected a similar result to Janke et al.[15] Any difference in washing procedures would not seem adequate to explain the large discrepancy in Zn content reported inside the QDs between our work and theirs, especially as we deliberately attempted to remove surface-bound ligands in the QD-TMEDA sample.

Thus, we hypothesized that the identity of indium and zinc carboxylate precursors utilized in the reaction may also play a role in dictating the efficiency of the Zn incorporation inside InP QDs. These precursors are typically prepared in situ in a one-pot reaction of In and Zn acetates with a desired carboxylic acid ("HX", where X is the desired carboxylate ligand for In and Zn metals) under vacuum at 100−150 °C and then reacted immediately with PTMS.[3,6,12,30] In these reactions, the amount of HX added is always less than needed to complex every In^{3+} and Zn^{2+} ion with 3 and 2 equiv of X^-, respectively, because any free acid causes broad size distributions.[31] Our (and other[6,30]) reactions always use 3 equiv of HX versus mole of $In(Ac)_3$, but with a Zn/In ratio of 1, a total of 5 equiv of HX would be required to fully convert the starting $In(Ac)_3$ and $Zn(Ac)_2$ to $In(X)_3$ and $Zn(X)_2$, respectively. Hence, heteroleptic $In(X)_x(Ac)_{3-x}$ and $Zn(X)_y(Ac)_{2-y}$ products with unknown x and y values are

DOI: 10.1021/acs.chemmater.9b04407
Chem. Mater. 2020, 32, 557−565

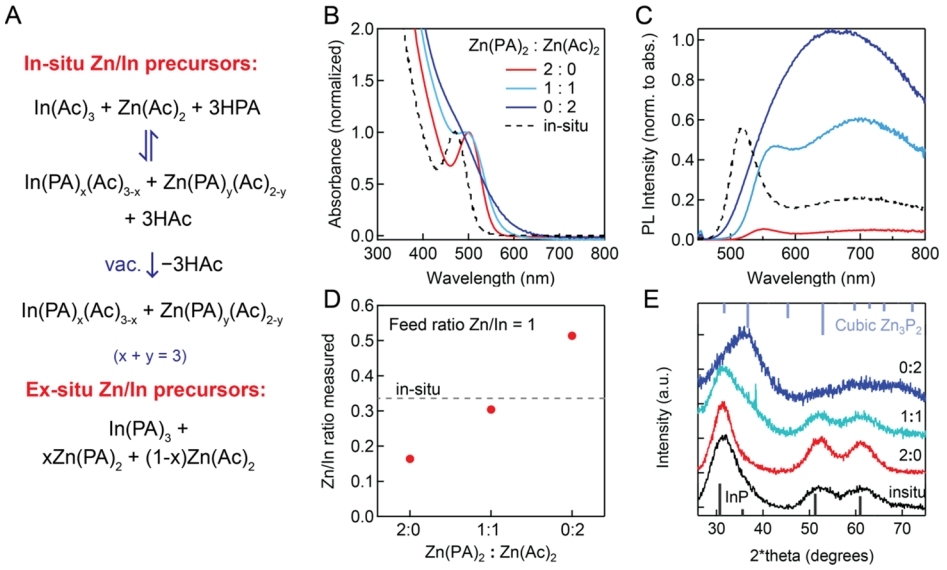

Figure 4. Controlling Zn incorporation into InP using Zn precursor reactivity. (A) Reaction scheme showing how forming precursors in situ with a deficit of palmitic acid leads to ill-defined precursor ligation. The bottom scheme shows ex situ precursor composition with well-defined ligation. HPA, protonated palmitic acid; HAc, protonated acetic acid. (B) Absorbance and (C) PL of samples made using in situ precursors and ex situ precursors with different $Zn(PA)_2/Zn(Ac)_2$ ratios. (D) Measured Zn/In ratio of washed QDs (from ICP-OES) as a function of $Zn(PA)_2/Zn(Ac)_2$ ratio. The in situ precursor result is shown as a dashed line. (E) XRD of same samples. The expected reflections are shown for zincblende InP (black lines at the bottom) and cubic Zn_3P_2 (blue lines at the top) for comparison.

expected (see reaction scheme in Figure 4A). Due to the fixed amount of HX, as the Zn/In ratio is varied, the proportion of acetate ligands will also vary. Furthermore, many researchers have opted to use different carboxylic acids (e.g., myristic,[31,32] palmitic,[3,30] or stearic[1] acid), or have made the indium carboxylate in situ from $In(Ac)_3$ and HX, but added separately prepared (ex situ-prepared) zinc carboxylates (e.g., zinc undecanoate,[1] stearate,[32] or oleate[9]) rather than $Zn(Ac)_2$.

With this in mind, we designed an experiment to test the effect that the zinc precursor ligation has on the resulting In(Zn)P QDs. We first prepared homoleptic Zn and In palmitates by metathesis reactions (see the Experimental Section) and then conducted a set of reactions with these ex situ precursors with the Zn/In ratio fixed to 1 but a varying ratio of $Zn(PA)_2/Zn(Ac)_2$. In each reaction, pure ex situ $In(PA)_3$ was used. We also performed a control experiment employing in situ-prepared precursors using a feed Zn/In ratio of 1 and 3 equiv of HPA (vs mole of In). The results are shown in Figure 4. All ex situ reactions show a red-shifted absorbance and, hence, larger QDs relative to the control in situ precursor case, where the In precursor is expected to have more acetate ligands. In a further control experiment, we varied the amount of palmitate and acetate ligands on $In(PA)_x(Ac)_{3-x}$ precursors in a pure InP reaction and also observed smaller QDs for higher proportions of acetate ligands on the In precursor (see Figure S11, Supporting Information). This effect can be attributed to an increased number of nuclei formed by $In(Ac)_3$ compared to $In(PA)_3$, indicating increased reactivity of acetate-ligated precursors. A higher reactivity of $Zn(Ac)_2$ versus $Zn(PA)_2$, or $In(Ac)_3$ versus $In(PA)_3$, is expected since the acetate precursors have a lower solubility in the solvent used for the synthesis (ODE), and hence, at a fixed concentration, the supersaturation will be higher. In addition, acetate precursors have a higher diffusion coefficient and will experience less steric hindrance when penetrating the ligand shell of the growing nuclei.[33]

For the ex situ precursor reactions, going from pure $Zn(PA)_2$ to pure $Zn(Ac)_2$, there is a considerable broadening of both the absorbance (Figure 4B) and PL (Figure 4C). We note that the optical changes are distinct from those observed by changes in the In precursor ligation alone (Figure S11). At the same time, the measured Zn/In ratio in washed QDs increases from 0.16 for pure $Zn(PA)_2$ to 0.51 for pure $Zn(Ac)_2$ (Figure 4D). Finally, XRD diffractograms in Figure 4E show that increasing the Zn content leads to a reduction in the InP (111) reflection at $2\theta = 30.7°$ and to an in-growth of a new reflection at $2\theta = 36.7°$, which indexes well to cubic Zn_3P_2 (220). There is also an apparent broadening of InP (220) and (311) reflections at $2\theta = 51.3°$ and 61°, respectively, with an increased Zn content. Indeed, the XRD pattern of the "full $Zn(Ac)_2$" sample matches better to cubic Zn_3P_2 (blue lines at the top of Figure 4E) than zincblende InP (black lines at the bottom of Figure 4E). The broad XRD reflections for the highest Zn content suggest that the InZnP QDs become more amorphous with the possible concomitant formation of the Zn_3P_2 crystal structure. The broad absorbance and PL of samples prepared with $Zn(Ac)_2$ are also reminiscent of broadened optical features reported for Zn_3P_2 QDs.[34]

These results strongly suggest that the ligation of Zn carboxylate precursors can affect the amount of Zn that is incorporated into QDs. When substituting $Zn(Ac)_2$ for $Zn(PA)_2$, changes in reactivity lead to more Zn incorporated into the bulk of the QDs during nucleation, evidenced by increased total zinc content, broadening of the optical features, and alteration of XRD reflections, all in a manner consistent with the formation of a product closer to Zn_3P_2 than InP.

The conclusion that the use of $Zn(Ac)_2$ leads to higher Zn content within the QD also explains the results obtained in the in situ precursor preparations reported in Figure 1. When a low Zn/In feed ratio is employed, at least some palmitate will be present on the heteroleptic $Zn(PA)_y(Ac)_{2-y}$ precursor, and the product remains InP-like with a blue-shift attributable to an

DOI: 10.1021/acs.chemmater.9b04407
Chem. Mater. 2020, 32, 557−565

altered band gap due to Zn alloying and/or smaller QDs due to the presence of some acetate ligands on the In precursor. At higher Zn/In feed ratios, the proportion of acetate ligands on Zn will be much greater, leading to a more Zn_3P_2-like product, which can explain the red-shifted and broadened optical features seen for a Zn/In ratio of >1.5 (see Figure 1A,B and our previous publication[3]). Indeed, XRD diffractograms of in situ precursor synthesis samples with high Zn/In ratios also exhibit reflections in line with Zn_3P_2 (see Figure S12, Supporting Information). Our results also suggest that inhomogeneity in the Zn content within an ensemble of QDs, evident through varying single-particle linewidths (Figure 1E) as well as varying single-QD lattice parameters (Figure 3G), could be attributed to variable ligation of heteroleptic Zn precursors.

In light of these results, it is hardly surprising that discrepancies in the observed structural and optical properties are observed in In(Zn)P QDs across the literature. Small changes in the Zn or In precursor ligation, induced deliberately or unintentionally via removal of acetic acid under vacuum degassing as well as differing complexation temperatures and times, can have marked effects on the amount and incorporation of Zn in the final QD product. This can easily be resolved by ensuring well-defined precursor ligation by using ex situ preparations for all precursors. Our results show that the incorporation of large amounts of Zn into the QD via more reactive Zn precursors results in undesirably broad optical features and an ill-defined crystal structure. Optimal spectral linewidths are in fact obtained using less reactive, homoleptic zinc precursors (e.g., $Zn(PA)_2$) where a large amount of Zn resides on the surface. A small lattice contraction is still observed in these cases (Figure 4E), which might afford better matching of lattices with ZnSe and ZnS shells while minimizing inhomogeneity arising from the incorporation of Zn_3P_2 domains via more reactive Zn precursors.

CONCLUSIONS

By using X-ray absorbance spectroscopy, we have proved that, for a typical synthesis, the majority of Zn found in In(Zn)P QDs is tightly bound to the nanocrystal surface as a Zn carboxylate species. However, by combining high-resolution HAADF-STEM with statistical parameter estimation, we have shown that a small amount of Zn is probably incorporated in the lattice of the QDs, evidenced by significant lattice contractions for some of the In(Zn)P QDs that we measured. Finally, we have shown that the amount of Zn incorporated into the QD lattice depends on the ligation, and hence reactivity, of the Zn precursor utilized during the synthesis. This result demonstrates that Zn must be present during the synthesis in a sufficiently reactive form to be incorporated into the InP QDs. Furthermore, the ill-defined ligation of the Zn precursor in common synthesis protocols can therefore explain varying single-QD emission linewidths and single-QD lattice parameters, as well as differences in results across the literature regarding the reported amount and location of Zn in In(Zn)P QDs.

EXPERIMENTAL SECTION

Materials. Indium(III) acetate anhydrate ($In(Ac)_3$, 99.99%), zinc(II) acetate anhydrate ($Zn(Ac)_2$, 99.99%), zinc phosphide (Zn_3P_2, ≥19% active phosphor basis, powder), palmitic acid (HPA, 99.99%, stored at −20 °C), tris(trimethylsilyl)-phosphine (PTMS, 95%), tetramethylenediamine (TMEDA, ≥98.5%), and 1-octadecene (ODE, 95%) were purchased from Sigma-Aldrich. All the chemicals were used without further purification.

Synthesis of Zinc Palmitate ($Zn(PA)_2$) Precursor. Fifteen milliliters of a 0.067 M solution of anhydrous Zn(acetate)$_2$ ($Zn(Ac)_2$) in methanol (total of 1 mmol of Zn) was added dropwise with vigorous stirring to 25 mL of a 0.08 M solution of sodium palmitate in methanol (total of 2 mmol of Na) in a 100 mL conical flask. A white precipitate formed ($Zn(PA)_2$). After 1 h of stirring, the precipitate was isolated by vacuum filtration, washed three times with methanol, dried under vacuum overnight, and stored in a nitrogen glovebox.

Synthesis of Indium Palmitate ($In(PA)_3$) Precursor. Ten millimoles of In(acetate)$_3$ and 40 mmol of palmitic acid were added to a round-bottom flask on a Schlenk line and held under vacuum for 1 h. The flask was then filled with nitrogen, and the contents were heated to 140 °C for 6 h. After this time, the $In(PA)_3$ product was precipitated by addition of acetone, filtered, washed with acetone (3 × 50 mL), and dried. The dried $In(PA)_3$ product was then mixed with another 40 mmol of palmitic acid, and the heating process was repeated again (140 °C, 6 h, N_2 atmosphere) to ensure complete replacement of all acetate ligands with palmitate. The final $In(PA)_3$ product was washed on a vacuum filter with 50 mL of acetone followed by 2 × 50 mL of a 1:1 hexane/acetone mixture, dried under vacuum overnight, and stored in a nitrogen-filled glovebox.

Synthesis of In(Zn)P QDs (in Situ Precursor Method). In(Zn)P QDs were synthesized following the method reported by our group.[7] In a typical reaction, 35 mg of $In(Ac)_3$ (0.12 mmol), a desired amount of $Zn(Ac)_2$ (the amount of which determines the feed Zn/In ratio), and 91 mg of palmitic acid (0.36 mmol) were added to a three-necked, round-bottom flask together with 7 mL of ODE. The mixture was held under vacuum (<10^{-1} mbar) overnight at 120 °C to remove oxygen, water, and acetic acid liberated from the in situ formation of indium and zinc palmitates. The solution was then heated to 300 °C under N_2 gas, at which point 17 μL of PTMS (0.06 mmol) in 1 mL of ODE was injected into the flask, resulting in the immediate formation of QDs. The QDs were grown for 1 h at 270 °C before cooling and washing three times via precipitation with methyl acetate and redispersion in toluene.

Synthesis of In(Zn)P QDs (ex Situ Precursor Method). In(Zn)P QDs were also synthesized using pre-prepared (ex situ) $Zn(PA)_2$ and $In(PA)_3$ precursors. In these reactions, 0.12 mmol of $In(PA)_3$ and a desired amount of $Zn(PA)_2$ were substituted for $In(Ac)_3$ and $Zn(Ac)_2$, respectively, and no palmitic acid was added. In some experiments, a mixture of $Zn(PA)_2$ and $Zn(Ac)_2$ was used. Otherwise, the procedure was identical to the in situ precursor method.

Growth of Larger In(Zn)P QDs for TEM. A growth stock solution of In and Zn palmitates was prepared in a round-bottom flask on a Schlenk line by mixing 0.5 mmol of $In(Ac)_3$, a desired amount of $Zn(Ac)_2$, and 1.5 mmol of palmitic acid in 6 mL of ODE. This mixture was heated to 120 °C overnight under vacuum and then to 250 °C under N_2 for 10 min and finally stored under N_2 at 100 °C. Separately, a PTMS growth stock solution was prepared in a N_2-filled glovebox by diluting 73 μL of PTMS (0.25 mmol) in 3 mL of ODE. After the formation of In(Zn)P QDs at 300 °C via the in situ method detailed above, the reaction temperature was lowered to 270 °C and held for 5 min. After this time, 2 mL of the In/Zn growth solution was added dropwise, and the PTMS stock solution was added to the reaction mixture over 3 h (1 mL/h) via a syringe pump. During this time, further 2 mL amounts of the In/Zn growth solution were added after 1 and 2 h of reaction time. After 3 h, or when the desired QD size was reached, the solution was cooled and washed as described above.

Treatment of In(Zn)P QDs with TMEDA. A dried powder of washed In(Zn)P QDs (~0.1−0.4 μmol of QDs) was suspended in 4 mL of neat TMEDA and stirred at 50 °C for 24 h in a nitrogen-filled glovebox. Following the TMEDA treatment, the QDs were washed three times via precipitation with methyl acetate and resuspension in toluene. The supernatant solution from washing containing TMEDA−ligand complexes was also kept for analysis.

Sample Characterization. UV−visible absorbance spectra were measured using a PerkinElmer Lambda 40 spectrometer. Photo-

DOI: 10.1021/acs.chemmater.9b04407
Chem. Mater. 2020, 32, 557−565

luminescence (PL) spectra were measured using an Edinburgh Instruments FLS980 spectrometer. X-ray diffractograms were obtained using a Bruker D8 Advance diffractometer. Inductively coupled plasma optical emission spectroscopy (ICP-OES) was carried out on QD samples dissolved in 3:1 (v/v) HCl/HNO_3 using an iCAP 6500 Thermo spectrometer (with a systematic error of ∼5%).

Extended X-ray Absorbance Fine Structure (EXAFS). Zn K-edge (9.6586 keV) EXAFS measurements were carried out at the Dutch−Belgian Beam Line (DUBBLE) at the European Synchrotron Radiation Facility (ESRF) in Grenoble, France.[35] The energy of the X-ray beam was controlled using a double-crystal monochromator operating in fixed-exit mode using a Si(111) crystal pair. Liquids ((In(Zn)P QDs in toluene, QD ligand−TMEDA solutions in methyl acetate, and zinc acetate standard in ethanol) were measured at 25 °C in 1 mm quartz capillaries. The zinc phosphide standard was measured at 25 °C as a powder dispersed in a cellulose pellet. All spectra were collected in transmission mode using Ar/He-filled ionization chambers at ambient temperature and pressure. Data extraction (normalization of raw signal, extraction of background, and Fourier transform) was conducted using Athena software[23] (see Table S1, Supporting Information, for details of data extraction and processing). EXAFS data were fit using Artemis software[23] (details of all fits in the Supporting Information).

HAADF-STEM and EDXS. High-resolution high-angle annular dark-field scanning transmission electron microscopy (HAADF-STEM) and energy dispersive X-ray spectroscopy (EDXS) measurements were performed using an aberration-corrected cubed FEI Titan electron microscope operated at 120 kV. EDXS spectra were acquired to determine the Zn/In atomic ratio. From the HAADF-STEM images, the lattice parameters inside the QDs were measured with high accuracy and precision by fitting a superposition of Gaussian functions to the atomic columns using StatSTEM software.[20] For lattice parameter quantification, only QDs that were oriented along a ⟨110⟩ zone axis were used, with focus on the planes, which correspond to the lattice parameter a (a, b, and c are identical since the structure is zincblende). To make sure that distances along the correct lattice planes were measured, Fourier transforms were calculated in each case. The obtained results from our STEM quantification approach, together with the error bars, are based on the raw data, and no prior calibration was used. To exclude any errors in the quantification related to instrumental mis-calibration, each sample was measured on the same day using the same microscope, high tension, pixel size, and magnification.

■ ASSOCIATED CONTENT

Supporting Information

The Supporting Information is available free of charge at https://pubs.acs.org/doi/10.1021/acs.chemmater.9b04407.

ICP results before/after TMEDA treatment; EXAFS data for TMEDA−Zn complexes and higher Zn content QDs; details of EXAFS data extraction and fitting and EXAFS data fits without Zn−P paths; and details of extraction of lattice parameters from atomic-resolution HRTEM images and optical characterization of the role of acetic acid on InZnP synthesis (PDF)

■ AUTHOR INFORMATION

Corresponding Authors

*E-mail: nrk@unimelb.edu.au (N.K.).
*E-mail: A.J.Houtepen@tudelft.nl (A.J.H.).

ORCID

Nicholas Kirkwood: 0000-0002-7845-7081
Thomas Altantzis: 0000-0002-4940-7931
Felipe V. Antolinez: 0000-0002-1787-0112
Freddy T. Rabouw: 0000-0002-4775-0859
Luca De Trizio: 0000-0002-1514-6358
Jaco J. Geuchies: 0000-0002-0758-9140
Jence T. Mulder: 0000-0002-4397-1347
Sara Bals: 0000-0002-4249-8017
Liberato Manna: 0000-0003-4386-7985
Arjan J. Houtepen: 0000-0001-8328-443X

Present Addresses

▽ARC Centre of Excellence in Exciton Science, School of Chemistry, The University of Melbourne, Parkville, Victoria 3052, Australia.
○Debye Institute for Nanomaterials Science, Utrecht University, 3584 CC Utrecht, The Netherlands.
◆Netherlands eScience Center, Science Park 140 (Matrix I), 1098 XG Amsterdam, The Netherlands.

Author Contributions

The manuscript was written through contributions of all authors. All authors have given approval to the final version of the manuscript.

Funding

A.J.H. acknowledges support from the European Research Council Horizon 2020 ERC grant agreement no. 678004 (Doping on Demand). This research is supported by the Dutch Technology Foundation TTW, which is part of The Netherlands Organization for Scientific Research (NWO) and is partly funded by the Ministry of Economic Affairs. S.B. acknowledges funding from the European Research Council (grant 815128 REALNANO). The authors gratefully acknowledge funding from the Research Foundation Flanders (FWO, Belgium) through project funding G.0381.16N and a postdoctoral grant to A.D.B. A.J.H., L.M., and J.M. acknowledge support from the H2020 Collaborative Project TEQ (grant no. 766900).

Notes

The authors declare no competing financial interest.

■ REFERENCES

(1) Xu, S.; Ziegler, J.; Nann, T. Rapid Synthesis of Highly Luminescent InP and InP/ZnS Nanocrystals. *J. Mater. Chem.* **2008**, *18*, 2653−2656.

(2) Xi, L.; Cho, D.-Y.; Besmehn, A.; Duchamp, M.; Grützmacher, D.; Lam, Y. M.; Kardynał, B. E. Effect of Zinc Incorporation on the Performance of Red Light Emitting InP Core Nanocrystals. *Inorg. Chem.* **2016**, *55*, 8381−8386.

(3) Pietra, F.; De Trizio, L.; Hoekstra, A. W.; Renaud, N.; Prato, M.; Grozema, F. C.; Baesjou, P. J.; Koole, R.; Manna, L.; Houtepen, A. J. Tuning the Lattice Parameter of In_xZn_yP for Highly Luminescent Lattice-Matched Core/Shell Quantum Dots. *ACS Nano* **2016**, *10*, 4754−4762.

(4) Dupont, D.; Tessier, M. D.; Smet, P. F.; Hens, Z. Indium Phosphide-Based Quantum Dots with Shell-Enhanced Absorption for Luminescent Down-Conversion. *Adv. Mater.* **2017**, *29*, 1700686.

(5) Chandrasekaran, V.; Tessier, M. D.; Dupont, D.; Geiregat, P.; Hens, Z.; Brainis, E. Nearly Blinking-Free, High-Purity Single-Photon Emission by Colloidal InP/ZnSe Quantum Dots. *Nano Lett.* **2017**, *17*, 6104−6109.

(6) Ramasamy, P.; Kim, N.; Kang, Y.-S.; Ramirez, O.; Lee, J.-S. Tunable, Bright, and Narrow-Band Luminescence from Colloidal Indium Phosphide Quantum Dots. *Chem. Mater.* **2017**, *29*, 6893−6899.

(7) Pietra, F.; Kirkwood, N.; de Trizio, L.; Hoekstra, A. W.; Kleibergen, L.; Renaud, N.; Koole, R.; Baesjou, P.; Manna, L.; Houtepen, A. J. Ga for Zn Cation Exchange Allows for Highly Luminescent and Photostable InZnP Based Quantum Dots. *Chem. Mater.* **2017**, *29*, 5192−5199.

DOI: 10.1021/acs.chemmater.9b04407
Chem. Mater. 2020, 32, 557−565

(8) Li, Y.; Hou, X.; Dai, X.; Yao, Z.; Lv, L.; Jin, Y.; Peng, X. Stoichiometry-Controlled Inp-Based Quantum Dots: Synthesis, Photoluminescence, and Electroluminescence. *J. Am. Chem. Soc.* **2019**, *141*, 6448−6452.
(9) Kim, Y.; Ham, S.; Jang, H.; Min, J. H.; Chung, H.; Lee, J.; Kim, D.; Jang, E. Bright and Uniform Green Light Emitting InP/ZnSe/ZnS Quantum Dots for Wide Color Gamut Displays. *ACS Appl. Nano Mater.* **2019**, *2*, 1496−1504.
(10) Chen, O.; Zhao, J.; Chauhan, V. P.; Cui, J.; Wong, C.; Harris, D. K.; Wei, H.; Han, H.-S.; Fukumura, D.; Jain, R. K.; Bawendi, M. G. Compact High-Quality CdSe-CdS Core-Shell Nanocrystals with Narrow Emission Linewidths and Suppressed Blinking. *Nat. Mater.* **2013**, *12*, 445−451.
(11) Boldt, K.; Kirkwood, N.; Beane, G. A.; Mulvaney, P. Synthesis of Highly Luminescent and Photo-Stable, Graded Shell CdSe/$Cd_xZn_{1-X}S$ Nanoparticles by in Situ Alloying. *Chem. Mater.* **2013**, *25*, 4731−4738.
(12) Xie, R.; Battaglia, D.; Peng, X. Colloidal InP Nanocrystals as Efficient Emitters Covering Blue to Near-Infrared. *J. Am. Chem. Soc.* **2007**, *129*, 15432−15433.
(13) Stein, J. L.; Mader, E. A.; Cossairt, B. M. Luminescent InP Quantum Dots with Tunable Emission by Post-Synthetic Modification with Lewis Acids. *J. Phys. Chem. Lett.* **2016**, *7*, 1315−1320.
(14) Laufersky, G.; Bradley, S.; Frécaut, E.; Lein, M.; Nann, T. Unraveling Aminophosphine Redox Mechanisms for Glovebox-Free InP Quantum Dot Syntheses. *Nanoscale* **2018**, *10*, 8752−8762.
(15) Janke, E. M.; Williams, N. E.; She, C.; Zherebetskyy, D.; Hudson, M. H.; Wang, L.; Gosztola, D. J.; Schaller, R. D.; Lee, B.; Sun, C.; Engel, G. S.; Talapin, D. V. Origin of Broad Emission Spectra in InP Quantum Dots: Contributions from Structural and Electronic Disorder. *J. Am. Chem. Soc.* **2018**, *140*, 15791−15803.
(16) Chan, L. Y.; Yu, K. M.; Ben-Tzur, M.; Haller, E. E.; Jaklevic, J. M.; Walukiewicz, W.; Hanson, C. M. Lattice Location of Diffused Zn Atoms in Gaas and InP Single Crystals. *J. Appl. Phys.* **1991**, *69*, 2998−3006.
(17) Mahajan, S.; Bonner, W. A.; Chin, A. K.; Miller, D. C. The Characterization of Highly-Zinc-Doped Inp Crystals. *Appl. Phys. Lett.* **1979**, *35*, 165−168.
(18) INSPEC, *Properties of Indium Phosphide*. The Institution of Engineering and Technology: The University of Michigan, 1991.
(19) Gómez, D. E.; van Embden, J.; Mulvaney, P. Spectral Diffusion of Single Semiconductor Nanocrystals: The Influence of the Dielectric Environment. *Appl. Phys. Lett.* **2006**, *88*, 154106.
(20) De Backer, A.; van den Bos, K. H. W.; Van den Broek, W.; Sijbers, J.; Van Aert, S. Statstem: An Efficient Approach for Accurate and Precise Model-Based Quantification of Atomic Resolution Electron Microscopy Images. *Ultramicroscopy* **2016**, *171*, 104−116.
(21) Ravel, B. Quantitative Exafs Analysis. In *X-Ray Absorption and X-Ray Emission Spectroscopy: Theory and Applications*; John Wiley & Sons, Inc., 2016, 281−302.
(22) Anderson, N. C.; Hendricks, M. P.; Choi, J. J.; Owen, J. S. Ligand Exchange and the Stoichiometry of Metal Chalcogenide Nanocrystals: Spectroscopic Observation of Facile Metal-Carboxylate Displacement and Binding. *J. Am. Chem. Soc.* **2013**, *135*, 18536−18548.
(23) Ravel, B.; Newville, M. Athena, Artemis, Hephaestus: Data Analysis for X-Ray Absorption Spectroscopy Using IFEFFIT. *J. Synchrotron Radiat.* **2005**, *12*, 537−541.
(24) Rehr, J. J.; Kas, J. J.; Vila, F. D.; Prange, M. P.; Jorissen, K. Parameter-Free Calculations of X-Ray Spectra with FEFF9. *Phys. Chem. Chem. Phys.* **2010**, *12*, 5503−5513.
(25) Tessier, M. D.; Baquero, E. A.; Dupont, D.; Grigel, V.; Bladt, E.; Bals, S.; Coppel, Y.; Hens, Z.; Nayral, C.; Delpech, F. Interfacial Oxidation and the Photoluminescence of InP-Based Core/Shell Quantum Dots. *Chem. Mater.* **2018**, *30*, 6877−6883.
(26) Stein, J. L.; Holden, W. M.; Venkatesh, A.; Mundy, M. E.; Rossini, A. J.; Seidler, G. T.; Cossairt, B. M. Probing Surface Defects of InP Quantum Dots Using Phosphorus Kα and Kβ X-Ray Emission Spectroscopy. *Chem. Mater.* **2018**, *30*, 6377−6388.
(27) Cros-Gagneux, A.; Delpech, F.; Nayral, C.; Cornejo, A.; Coppel, Y.; Chaudret, B. Surface Chemistry of InP Quantum Dots: A Comprehensive Study. *J. Am. Chem. Soc.* **2010**, *132*, 18147−18157.
(28) van der Stam, W.; Geuchies, J. J.; Altantzis, T.; van den Bos, K. H. W.; Meeldijk, J. D.; Van Aert, S.; Bals, S.; Vanmaekelbergh, D.; de Mello Donega, C. Highly Emissive Divalent-Ion-Doped Colloidal $CsPb_{1-X}M_xBr_3$ Perovskite Nanocrystals through Cation Exchange. *J. Am. Chem. Soc.* **2017**, *139*, 4087−4097.
(29) Hassinen, A.; Moreels, I.; De Nolf, K.; Smet, P. F.; Martins, J. C.; Hens, Z. Short-Chain Alcohols Strip X-Type Ligands and Quench the Luminescence of PbSe and CdSe Quantum Dots, Acetonitrile Does Not. *J. Am. Chem. Soc.* **2012**, *134*, 20705−20712.
(30) Kim, S.; Kim, T.; Kang, M.; Kwak, S. K.; Yoo, T. W.; Park, L. S.; Yang, I.; Hwang, S.; Lee, J. E.; Kim, S. K.; Kim, S.-W. Highly Luminescent InP/GaP/ZnS Nanocrystals and Their Application to White Light-Emitting Diodes. *J. Am. Chem. Soc.* **2012**, *134*, 3804−3809.
(31) Gary, D. C.; Cossairt, B. M. Role of Acid in Precursor Conversion During InP Quantum Dot Synthesis. *Chem. Mater.* **2013**, *25*, 2463−2469.
(32) Li, L.; Reiss, P. One-Pot Synthesis of Highly Luminescent InP/ZnS Nanocrystals Without Precursor Injection. *J. Am. Chem. Soc.* **2008**, *130*, 11588−11589.
(33) de Nolf, K.; Capek, R. K.; Abe, S.; Sluydts, M.; Jang, Y.; Martins, J. C.; Cottenier, S.; Lifshitz, E.; Hens, Z. Controlling the Size of Hot Injection Made Nanocrystals by Manipulating the Diffusion Coefficient of the Solute. *J. Am. Chem. Soc.* **2015**, *137*, 2495−2505.
(34) Glassy, B. A.; Cossairt, B. M. Resolving the Chemistry of Zn_3P_2 Nanocrystal Growth. *Chem. Mater.* **2016**, *28*, 6374−6380.
(35) Borsboom, M.; Bras, W.; Cerjak, I.; Detollenaere, D.; Glastra van Loon, D.; Goedtkindt, P.; Konijnenburg, M.; Lassing, P.; Levine, Y. K.; Munneke, B.; Oversluizen, M.; Van Tol, R.; Vlieg, E. The Dutch-Belgian Beamline at the ESRF. *J. Synchrotron Radiat.* **1998**, *5*, 518−520.

DOI: 10.1021/acs.chemmater.9b04407
Chem. Mater. 2020, 32, 557−565